WARSAW UNIVERSITY OF TECHNOLOGY Index 351733
FACULTY OF CIVIL ENGINEERING
COMMITTEE FOR CIVIL AND WATER ENGINEERING
POLISH ACADEMY OF SCIENCES ISSN 1230-2945
DOI: 10.24425/ace.2024.149876
ARCHIVES OF CIVIL ENGINEERING
Vol. LXX ISSUE 2 2024
pp. 477 –492

Research paper

Buttress wall in limiting wall deformation caused by deep excavation: A case study for colluvial soil in Vietnam

Luc Manh Bui[1], Li Wu[2], Minh Ngoc Do[3], Yao Cheng[4], Dao Jun Dong[5]

Abstract: The objective of this study is to assess the impact of utilizing a BW (Buttress wall) to control the deflection of a diaphragm wall in colluvial soil conditions in Vietnam. The physical and mechanical properties of the colluvial layers are evaluated using data closely monitored during a specific project, serving as validation for 3D numerical simulations utilizing the Hardening Soil Model. The analysis results closely match the field monitoring data, which has tested the accuracy of the simulation model. This forms the basis for further investigations into the dimensional parameters of BW walls, including length, thickness, and spacing between them. The results obtained from the parametric study demonstrate that altering the wall length and spacing between BW walls significantly limits the deflection of the diaphragm wall, while changes in thickness have a negligible effect. Through the 3D numerical simulations, a linear relationship between the maximum wall deflection and parameters such as wall length and spacing between BW walls has been established.

Keywords: buttress wall, colluvial soil, deep excavation, numerical analysis, limiting wall deformation

[1]PhD student, Eng., Faculty of Engineering, China University of Geosciences (Wuhan), No. 388 Lumo Road, Wuhan 430074, Hubei, China, e-mail: lucbui.uctgeo@gmail.com, ORCID: 0009-0006-7816-8796
[2]Prof., PhD., Eng., Doctoral supervisor, Faculty of Engineering, China University of Geosciences (Wuhan), No. 388 Lumo Road, Wuhan 430074, Hubei, China, e-mail: lwu@cug.edu.cn, ORCID: 0000-0001-9651-3772
[3]Eng., Doctoral supervisor, Department of Geotechnical Engineering, Civil Engineering Faculty, University of Transport Technology, No. 54 Trieukhuc Road, Hanoi, Vietnam, e-mail: ngocdm@utt.edu.vn, ORCID: 0009-0007-8198-0985
[4]Assoc. Prof., PhD., Eng., Doctoral supervisor, Faculty of Engineering, China University of Geosciences (Wuhan), No. 388 Lumo Road, Wuhan 430074, Hubei, China, e-mail: chengyao@cug.edu.cn, ORCID: 0000-0003-2925-2773
[5]Assoc. Prof., PhD., Eng., Doctoral supervisor, Faculty of Engineering, China University of Geosciences (Wuhan), No. 388 Lumo Road, Wuhan 430074, Hubei, China, e-mail: 66826130@qq.com, ORCID: 0009-0005-9055-5564

1. Introduction

Rapid urbanization requires deep excavation for underground works as ground space becomes limited. The challenge of deep excavation is great due to the need to minimize the displacement of adjacent ground which is unpredictable due to continuous changes in engineering geological conditions [1, 2].

The current reality highlights various methods to control displacement during deep excavation construction [3–14]. One such method is the installation of buttress walls [12, 13, 15, 16]. Notably, this method has become popular in Taiwan and Singapore, proving effective in minimizing retaining wall deformation. Previous research [15–17] has also elucidated the mechanical properties of buttress walls (BW) and their impact on limiting diaphragm wall displacement, but these studies mainly focused on excavations in soft soil conditions within urban areas; there have not been many studies on the use of buttress walls in the colluvial soil, which is often found in urban areas in Northern Vietnam.

This paper explores the physical and mechanical characteristics of cumulus soil layers. By comparing on-site monitoring data with effectively implemented numerical models for a specific project, the article conducts a series of parametric studies investigating the distance, length, and thickness of buttress walls. The goal is to clarify how these parameters influence the deformation of diaphragm walls in this context.

2. Study site

2.1. Project background and soil descriptions

2.1.1. Project background

The case discussed in this article pertains to a 22-storey 5-star hotel featuring a reinforced concrete frame structure supported by a bored pile foundation system. The diaphragm walls surrounding the building on the east, west, and north sides stand at a height of 26 meters. Originally, the BW system was engineered to serve the dual purpose of providing support and minimizing diaphragm wall deformation, while also being an integral part of the building's structural framework (Fig. 1). However, due to aesthetic considerations for the hotel project, the BW wall system will be dismantled, and the responsibility for supporting the diaphragm wall will be taken over by the anchor system (Table 1). The north wall area has been selected for research in this study, primarily due to its extensive length and its proximity to critical elements such as road systems, underground cable systems, drainage systems, and densely populated residential area (Fig. 1).

The cross-section of the excavation is shown in Figure 2. The diaphragm wall, 0.6 m thick and 26 m long, is used as a soil retaining system. The compressive strength of concrete (f_c') of the diaphragm wall is 25 MPa. The BWs are built after completing the construction of the main diaphragm walls. Ground anchors are arranged in 5 layers with specific lengths as shown in Figure 2.

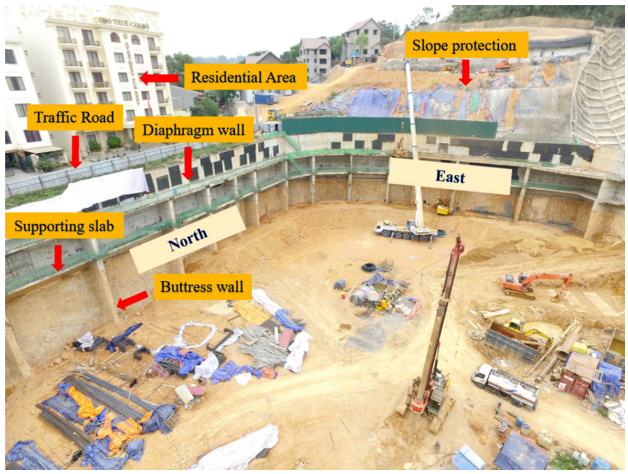

Fig. 1. Photo of the excavation site

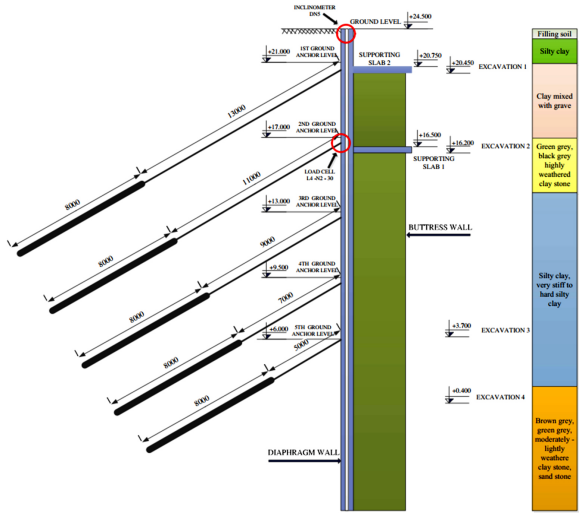

Fig. 2. Typical section

A system of monitoring points for diaphragm wall displacement has been set up, comprising 12 monitoring points (Fig. 3). Monitoring point DN1 is specifically installed for monitoring the diaphragm wall in the East area. Monitoring points DN2-DN7 have been placed to track the displacements of the diaphragm wall in the northern area, while points DN8-DN12 are designated for monitoring the displacements of the diaphragm wall in the western area. Additionally, for the purpose of monitoring anchor forces during construction, a system of 4 anchor points has been strategically positioned in the northern area, namely L4-N2-30, and L3-N2-45, and in the East area, denoted as L2-N2-46 and L1-N2-58.

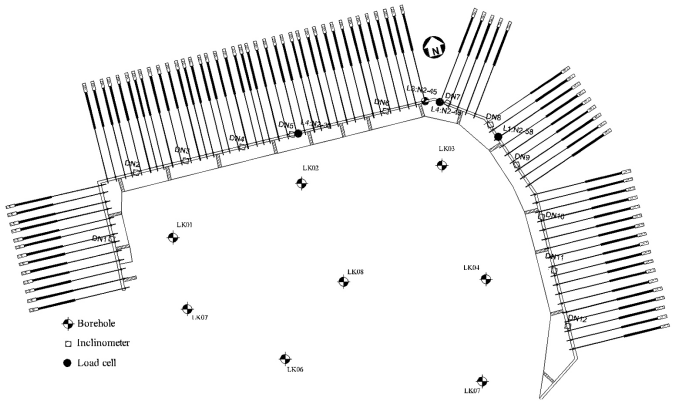

Fig. 3. Position of the observation instrument

The construction process is divided into 9 stages as shown in Table 1.

Table 1. Construction steps of the excavation

Phase	Construction sequences
1	Diaphragm wall installation
2	Excavation 1
3	Buttress wall installation, construction supporting slab 1
4	Excavation 2
5	Construction supporting slab 2
6	Excavation 3
7	Anchor installation
8	Excavation 4
9	Demolished buttress wall

2.1.2. Soil descriptions

To clarify the geological conditions of the study area, 8 boreholes are numbered LK01 to LK08 with depths ranging from 41 m to 50 m. These boreholes provide information about the distribution of soil layers. Along with that, SPT testing is performed during the drilling process, the distance is 2 m for each test. Disturbed and undisturbed soil samples and rock samples are sent to the laboratory to determine physical characteristics and particle composition, thereby classifying the soil and rock. To determine the mechanical properties, oedometer test, direct shear test and trixial test were performed. The distribution, physical properties, and strength parameters of the soil layers can be found in Table 3.

The uppermost layer is the backfill layer, which is predominant in most survey boreholes. It has a thickness ranging from 0.5 m to 6 m, with an average thickness of 3 m. This layer is characterized by yellow-grey and yellow-brown mixed clay, interspersed with gravel, boulders, and concrete. Immediately below is a hard plastic to semi-hard clay layer, featuring yellow-brown and pink-brown mixed clay. This layer contains numerous gravels and ranges in thickness from 1.2 m to 9.6 m, with SPT test results varying from 7 to 38. Following this layer is a clay layer, mixed with shades of yellow-brown and yellow-gray, exhibiting a semi-hard to hard state and containing substantial grit. Its thickness varies from 3.4 m to 19.0 m, with SPT index values ranging from 11 to 62. Beneath it is a layer of gray siltstone, dark gray, and strongly weathered, with thickness ranging from 1.4 m to 5.2 m and SPT test results from 32 to 50.

The subsequent layer consists of clay mixed with yellow-brown and yellow-gray, displaying a hard plastic to semi-hard state and mixed with successive grits. Its thickness ranges from 3.8 m to 5.5 m, with SPT experiments yielding results from 8 to 19. Finally, the geological survey reports a silty clay layer, which is gray, dark gray, and strongly weathered, with an SPT index greater than 50. It's worth noting that there is no groundwater in the survey area.

These soil layers are formed by the process of erosion, transport and accumulation of temporary flows. The common characteristics of these soil types are their complex and heterogeneous composition, often mixed with debris, rocks, and irregular particle sizes. The material particles are characterized by their sharp edges, substantial porosity, high shrinkage tendencies, low adhesive forces, and a propensity to disintegrate rapidly when exposed to water flow. Detailed physical property parameters can be referenced in Figures 4, 5, and 6.

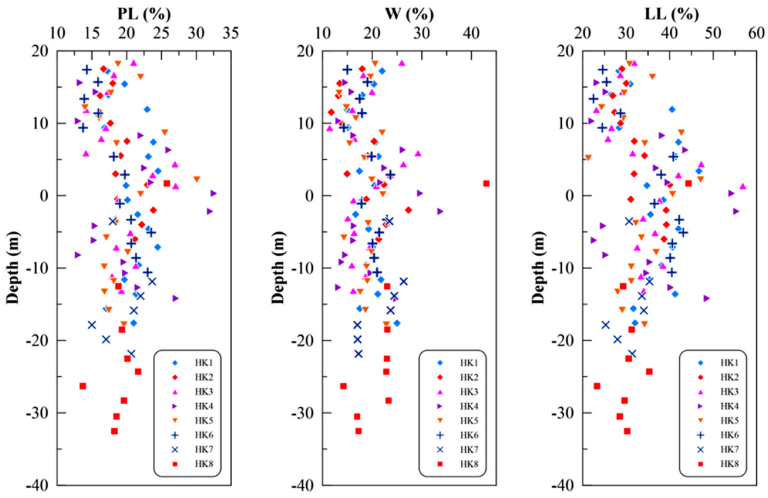

Fig. 4. Information from drilling hole: PL, moisture content (w), LL

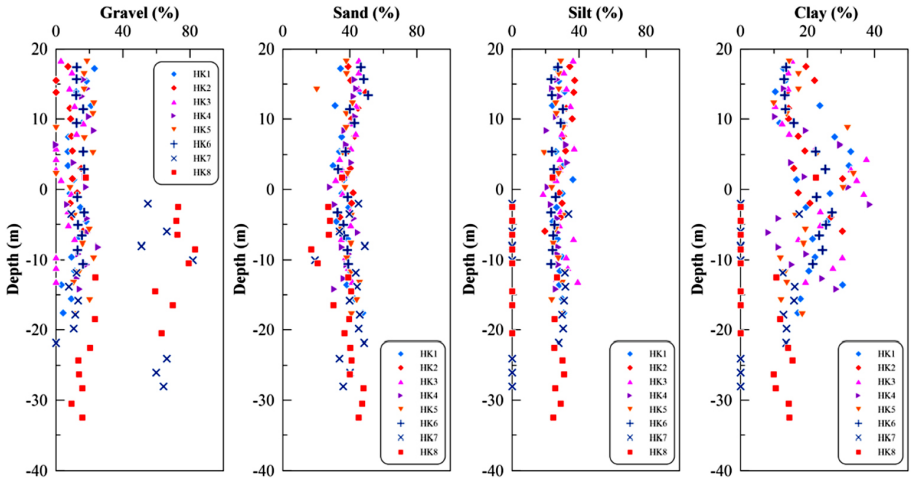

Fig. 5. Information from drilling hole: Particle size determination

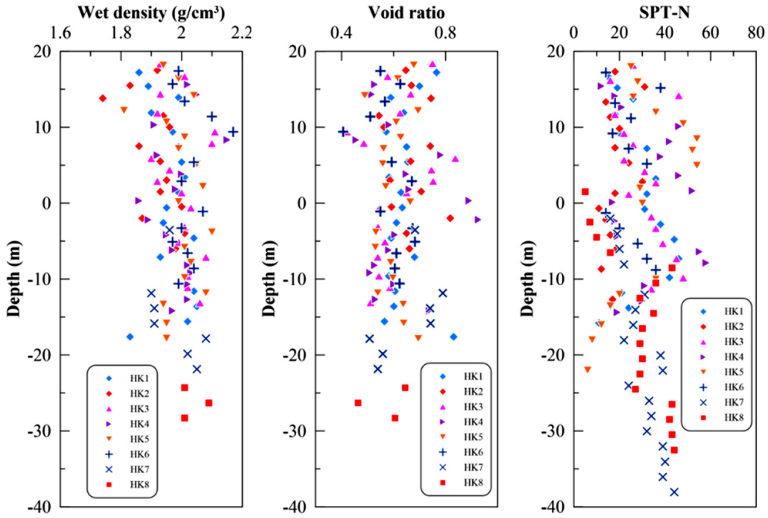

Fig. 6. Information from drilling hole: Wet density, void ratio, SPT-N

2.2. Numerical model

The primary numerical analysis tool employed in this study is the three-dimensional finite element computer program, Plaxis 3D (2018). Given that the northern retaining wall block is not only the longest but also adjacent to densely populated areas, as well as the road and drainage system, it was chosen for the confirmation analysis. For simplification purposes, the study will model the wall block at monitoring points DN5 and L4-N2-30.

Figure 7 illustrates the finite element mesh utilized for analysis, featuring a total of 40,880 elements and 67,100 nodes. To simulate soil behavior under both undrained and drained conditions, the Hardening Soil Model (HS Model) [18] was adopted.

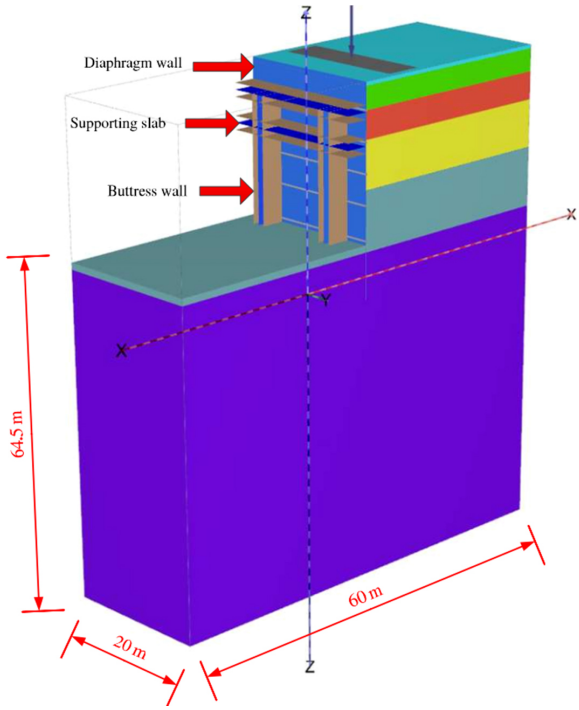

Fig. 7. FE model of the excavation

The HS model requires secant stiffness parameters (E_{50}^{ref}) corresponding to the reference stress, pref, tangential reference stiffness for the main line gauge load ($E_{\text{oed}}^{\text{ref}}$), unloaded reference stiffness/ reload ($E_{\text{ur}}^{\text{ref}}$) and strength to stress-level dependent of stiffness (m). According to [19] $p^{\text{ref}} = 100$ kPa, m is set equal to 1. E_{50}^{ref} and $E_{\text{oed}}^{\text{ref}}$ can be estimated according to [20] $E_{50}^{\text{ref}} = E_{\text{ur}}^{\text{ref}}/3$, $E_{\text{oed}}^{\text{ref}} = E_{50}^{\text{ref}}$. Based on the unconfined compression test in the laboratory, the hardness $E_{\text{oed}}^{\text{ref}}$ was found, the results are as shown in Table 2. For the deepest layer, the recorded SPT index is greater than 50, based on the studies of Hsiung [21] and Yong [22], the Eoed value is taken in the range of 2000·NSPT–4000·NSPT kPa. Hence for this layer, the Eoed value is assumed to be 2500·NSPT with NSPT = 80. Among other HS parameters, unit weight of soil (γ_t) obtained from testing undisturbed samples, effective cohesion (c') and the effective internal friction angle ($\phi\prime$) (Except for the Filling soil layer and the deepest layer which are assumed) obtained from trixial test. According to Bolton (1986), the expansion angle (ψ) can be approximately equal to $\psi = \phi\prime - 300$ for sandy soils. However, for values of $\phi\prime$ less than 300, ψ is almost zero for clays. The Poisson ratio for the unloading-reloading state (ν_{ur}) can be reasonably assumed to be 0.2 and the damage coefficient (R_f) is set to 0.9.

Table 2. Input parameters of the HS model

Soil layer	Filling soil	Silty clay, plasticity stiff – semi stiff	Clay mixed with gravel, semi stiff – stiff	Green grey, black grey highly weathered clay stone	Silty clay, very stiff to hard silty clay	Brown grey, green grey, moderately – lightly weathere clay stone, sand stone.
Thickness (m)	0.5	3	3.7	6.3	7.9	43.1
Drainage type	Drained	Undrained (A)	Undrained (A)	Drained	Undrained (A)	Drained
γ_t (kN/m^3)	17.5	20.4	20.2	20.9	20.7	26.9
N-spt	7	22.5	36.5	40	38.5	> 5
E_{50}^{ref} (kPa)	10000	18330	17740	27110	24370	200000
$E_{\mathrm{oe}}^{\mathrm{ref}}$ (kPa)	10000	18330	17740	27110	24370	200000
$E_{\mathrm{ur}}^{\mathrm{ref}}$ (kPa)	30000	54990	53220	81330	73110	600000
m	1	1	1	1	1	0.5
c'	5	18.7	27.5	30.9	31.3	160
ϕ'	25	29.8	39.6	35.9	37.5	35
ψ	–	–	–	5.9	7.5	5
v_{ur}	0.2	0.2	0.2	0.2	0.2	0.2
R_{inter}	0.7	0.65	0.65	1	1	1

Table 3. Diaphragm wall parameters

Structure	Material model	Drainage type	d (m)	E (kPa)	v
Buttress Wall	Elastic	Non-porous	0.6	2.65E+07	0.2
Supporting slab	Elastic	Non-porous	0.3	2.65E+07	0.2
Diaphragm wall	Elastic	Non-porous	0.6	2.65E+07	0.2

Table 2 summarizes the parameters of the soil types used in the analysis for structural elements such as diaphragm walls, retaining walls, transverse walls, and concrete floor slabs, which are part of the top-down construction method, they are modeled as slab elements and simulated as linear elastic materials. Poisson's ratio for concrete is set to 0.15. The Young's modulus of concrete (E_c) is estimated following the recommendations by the American Concrete Institute [23]. The interface element is used to model the ground plate element's interaction behavior. The interface friction between the structural elements and the adjacent soil is assumed to follow the Mohr-Coulomb model [15, 24], with its value is expressed as a reduction factor intensity (R_{inter}). In addition, the anchor cable and anchor bonding parameters are also provided in Table 4.

Table 4. Anchor parameters

Element	Material type	EA	E (kPa)	D (m)
Bonding part	Elastic	–	3.25E+07	0.16
Cable	Elastic	7.90E+04		

2.3. Comparison of mesurement data and simulation results

Through comparing the results of monitoring and analyzing wall deflections using the finite element method during the excavation stages, it shows that the analysis results agree well with observed data (Fig. 8). During excavation stages 1 and 2, where the excavation

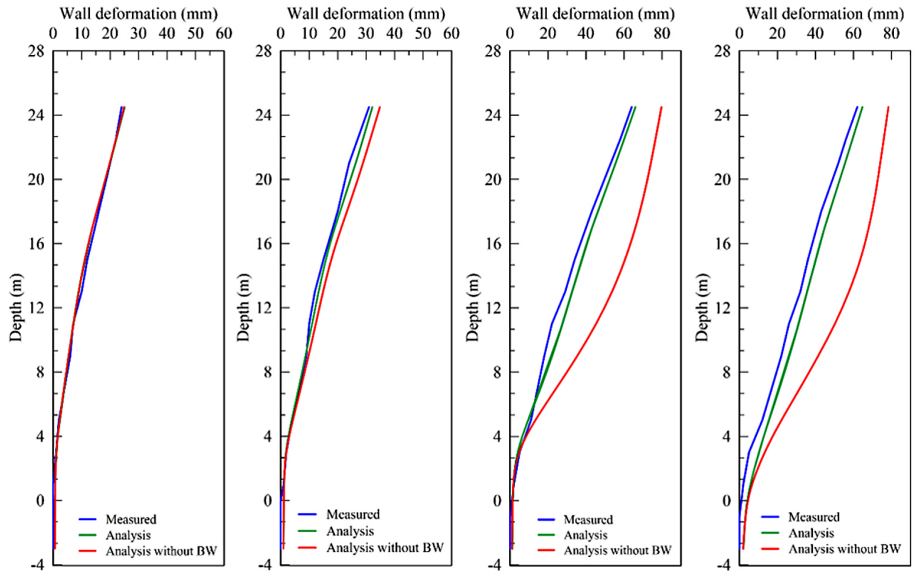

Fig. 8. Comparison of wall deformation from field observation and from analysis

depth is relatively shallow, the resulting diaphragm wall deformation is small. However, in excavation stages 3 and 4, with deeper excavation depths, the wall deformation increases accordingly. It's worth noting that the largest deviation between observed data and simulation results is only 3%.

In addition, an analysis was conducted assuming the absence of BW to compare wall deflection. The results from this analysis without BW walls are also consistent with the findings by Ou et al. 1993 [25]. Therefore, the employed simulation methodology has been validated and can be applied to the subsequent numerical analyses discussed in the following section.

Based on the aforementioned comparison results, it is evident that the presence of BWs leads to reduced wall deflection compared to when they are not installed. Specifically, the deflection of the wall is reduced by about 20% when using BWs, proving their effectiveness in minimizing the displacement of the diaphragm wall during excavation construction.

According to Figure 9, all field measurement results and finite element analysis show an increase in anchor force with pre-load, confirming that the anchor has contributed to reducing the displacement of diaphragm walls. The analysis indicates that the anchor force increases from phase 8 to phase 9 because the diaphragm wall relies entirely on the anchor system to limit displacement. The measurement process for the actual anchor force is conducted at an unspecified time from stage 8 to stage 9. However, it is apparent that the measurement results align with the range of anchor force analyzed during phases 8 and 9. This demonstrates that the finite element method can simulate the working of structural components with reliable accuracy.

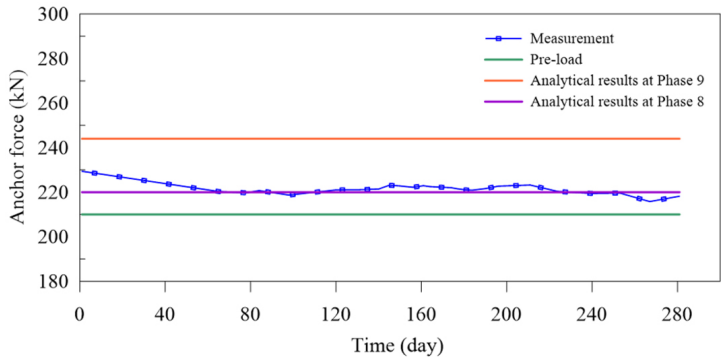

Fig. 9. Comparison of anchor force from field observation and from analysis

3. Effect of buttress on wall deformation

3.1. Parameters of buttress

The results obtained from the previously verified model serve as the foundation for the numerical analyses conducted in this section. The hypothetical excavation scenario is outlined as follows: The excavation has a constant depth and utilizes a retaining wall with a thickness of 0.6 m (t_{DW}), a 26 m deep soil retaining structure (H_t), and a braced

floor with a thickness (t_{slab}) of 0.3 m. The concrete used for both of these elements has a compressive strength (f'_c) of 25 MPa. The construction phase is carried out in 9 steps as shown in Table 1.

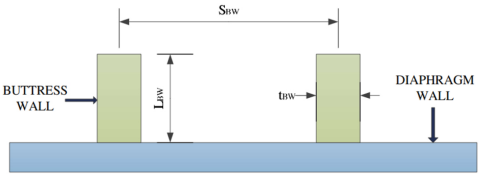

Fig. 10. Plan of the hypothetical excavation

The dimensions and other parameters of the used anchors are the same as in the above simulations. The depth and compressive strength (f'_c) of the buttress wall are set in the same as the diaphragm wall manner. The soil layers are assumed to possess the distribution and properties as described in Table 2, with a simulated depth extending up to 40 meters.

For the parametric study, the values of L_{BW}, t_{BW}, S_{BW}, H_{BW} are shown in Table 5. Notably, when $L_{BW} = 0$ or $t_{BW} = 0$, it signifies that the excavation is not constructed with a buttress wall.

Table 5. Basic values of parameters and variations applied in the parametric studies

Parameters	Basic value	Variation value
L_{BW} (m)	3.2	0; 5; 10; 15
t_{BW} (m)	0.6	0; 0.2; 0.4; 0.8; 1; 1.2
S_{BW} (m)	11.7	0; 2.5; 5; 15; 20

3.2. Results and discussion

3.2.1. Effect of the buttress wall length

The impact of enhancing the flexural stiffness of the buttress wall by increasing LBW is clearly evident in the reduction of diaphragm wall deflection.

The limitation of diaphragm wall displacement is not readily apparent when altering the length of the Buttress Wall in excavation steps 1 and 2. However, there is a significant disparity in excavation steps 3 and 4 (Fig. 11). For instance when the length of the BW wall is set at 15 meters, the diaphragm wall deflection is reduced by as much as 68% compared to the scenario where no BW wall is installed.

Figure 12 illustrates that the maximum displacement of the diaphragm wall exhibits an inverse relationship with the wall length. As the diaphragm wall length increases, the deflection of the wall decreases; however, this relationship does not follow a linear pattern. When modifying the wall length from 3.2 meters to 5 meters, the maximum displacement of the diaphragm wall is reduced by 47%. In contrast, when extending the wall length from 5 meters to 10 meters and 15 meters, the maximum displacement of the diaphragm wall does not decrease significantly.

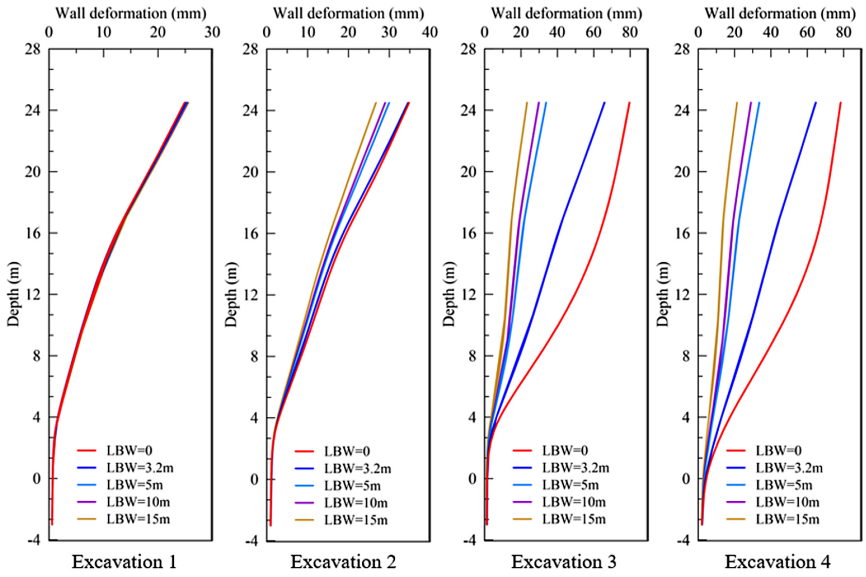

Fig. 11. The wall deformations under different length of buttress wall

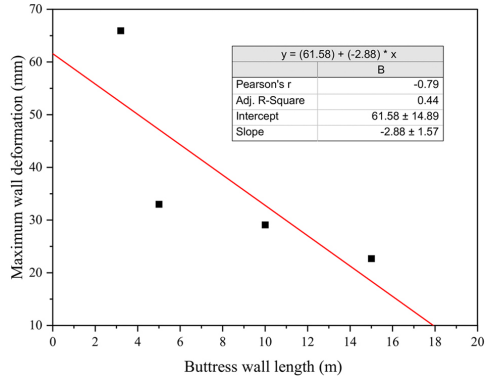

Fig. 12. The maximum wall deformations with buttress wall length

3.2.2. Effect of the spacing between buttress wall

In theory, decreasing the spacing between buttress walls has the potential to reduce the overall deflection of the wall. Therefore, determining the appropriate distance between buttress walls to achieve the objective of minimizing wall deflection presents a challenge for engineers. In order to grasp the impact of the spacing between wall piers, this study carried out an analysis for varying S_{BW}. The range of S_{BW} adjustments is outlined in Table 3.

Figure 13 illustrates the impact of reducing the spacing between buttress walls on wall deflection. The reduction in deflection is not prominently noticeable during excavation steps 1 and 2. However, in excavation steps 3 and 4, the influence of narrowing the gap between but-

tress walls becomes evident in reducing wall deflection. The variation in wall deflection when the inter-BW distance is 11.7 meters and 15 meters is relatively modest. The difference in deflection between the widest and narrowest inter-BW distances falls within the range of 30%.

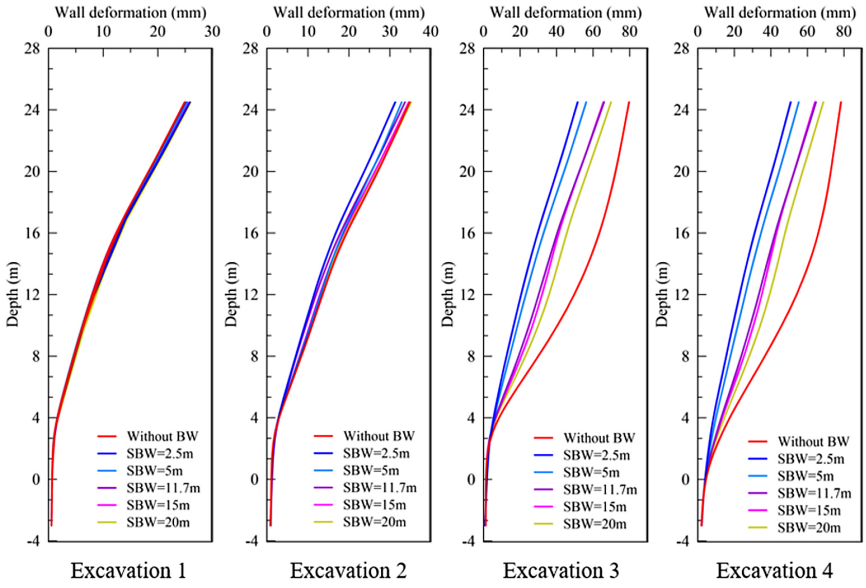

Fig. 13. The wall deformations under different spacing between buttress wall

Figure 14 further demonstrates that the maximum displacement (δ_{hm}) of the wall is directly proportional to the distance between the buttress walls (BW). As the BW distance increases, the maximum wall deflection also increases, following an approximately linear relationship described by the following function: $\delta_{hm} = 1.03 \cdot S_{\mathrm{BW}} + 50.60$ mm.

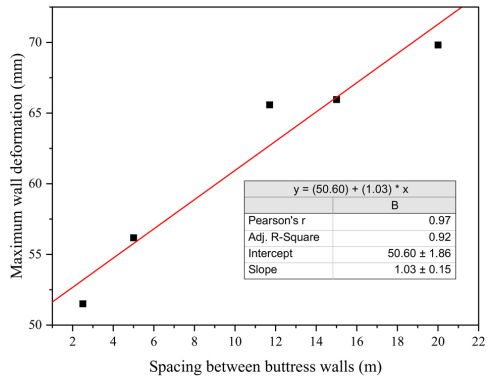

Fig. 14. The maximum wall deformations with spacing between buttress walls

3.2.3. Effect of the thickness of buttress

In theory, as the thickness of the Buttress Wall (t_{BW}) increases, the bending stiffness of the retaining system involving the diaphragm wall and buttress wall should also increase, leading to a reduction in deflection.

However, as depicted in Figure 15, the increase in t_{BW} results in a reduction in deflection that is nearly negligible. In this particular case, values larger than $t_{BW} = 0.8$ meters have minimal impact on reducing wall deflection.

Furthermore, Figure 16 demonstrates that the maximum displacement of the diaphragm wall is inversely proportional to the thickness of the buttress wall (t_{BW}). As the thickness of the BW wall increases, the deflection of the diaphragm wall decreases approximately linearly, as described by the following formula: $\delta_{hm} = 74.08 - 12.93 \cdot t_{BW}$ mm.

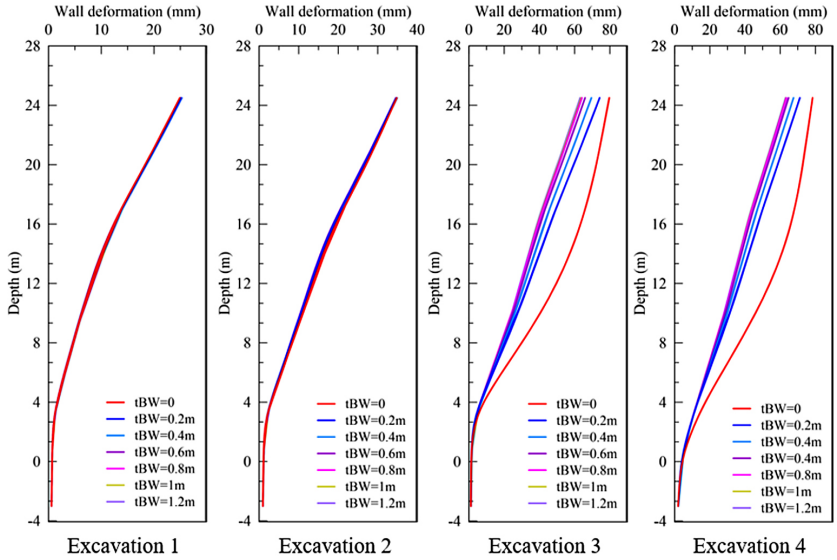

Fig. 15. The wall deformations under different thickness of buttress wall

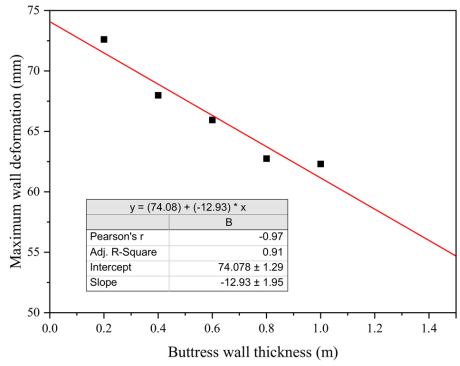

Fig. 16. The maximum wall deformations with buttress wall thickness

4. Conclusions

Based on the findings presented in this paper, the following conclusions can be drawn:

1. The Buttress Wall (BW) method is well-suited for limiting diaphragm wall deflection in colluvial soil conditions in Vietnam.
2. The influence of increasing BW wall thickness on diaphragm wall deflection is minimal. The maximum wall deviation is inversely proportional to the BW wall thickness, as described by the formula: $\delta_{hm} = 74.08 - 12.93 \cdot t_{\mathrm{BW}}$ mm.
3. When the BW wall has a fixed length, reducing the spacing between BW walls effectively reduces diaphragm wall deformation. The maximum wall deflection of the diaphragm wall is inversely proportional to the distance between BW walls, following the formula: $\delta_{hm} = 1.03 \cdot S_{\mathrm{BW}} + 50.60$ mm.
4. The length of the BW wall has a significant impact on limiting diaphragm wall deflection. However, when the BW wall length exceeds 5 meters, the maximum wall deflection tends to decrease slowly. The relationship between maximum diaphragm wall deflection and BW wall length is not linear.

References

[1] J.F. Zhang, J.J. Chen, J.H. Wang, and Y.F. Zhu, "Prediction of tunnel displacement induced by adjacent excavation in soft soil", *Tunnel and Underground Space Technology*, vol. 36, pp. 24–33, 2013, doi: 10.1016/j.tust.2013.01.011.

[2] M.G. Li, J.H. Wang, J.J. Chen, and Z.J. Zhang, "Responses of a newly built metro line connected to deep excavations in soft clay", *Journal of Performance of Construction Facilities*, vol. 31, no. 6, 2017, doi: 10.1061/(ASCE)CF.1943-5509.0001091.

[3] R.P. Chen, F. Meng, Z.C. Li, Y. Ye, and J. Ye, "Investigation of response of metro tunnels due to adjacent large excavation and protective measures in soft soils", *Tunnel and Underground Space Technology*, vol. 58, pp. 224–235, 2016, doi: 10.1016/j.tust.2016.06.002.

[4] M.G. Li, Z.J. Zhang, J.J. Chen, J.H. Wang, and A.J. Xu, "Zoned and staged construction of an underground complex in Shanghai soft clay", *Tunnel and Underground Space Technology*, vol. 67, pp. 187–200, 2017, doi: 10.1016/j.tust.2017.04.016.

[5] A.R. Gaba, "Jet grouting at Newton station", in *Proceedings of the 10th Southeast Asia Geotechnical Conference*. Taipei, 1990, pp. 77–79.

[6] G.B. Liu, C.W. Ng, and Z.W. Wang, "Observed performance of a deep multistrutted excavation in Shanghai soft clays", *Journal of Geotechnical and Geoenvironmental Engineering*, vol. 131, no. 8, pp. 1004–1013, 2005, doi: 10.1061/(ASCE)1090-0241(2005)131:8(1004).

[7] S. Parashar, R. Mitchell, M.W. Hee, D. Sanmugnathan, E. Sloan, and G. Nicholson, "Performance monitoring of deep excavation at Changi WRP project, Singapore", in *Proceedings of the 7th International Symposium on Field Measurements in Geomechanics*. ASCE,2007, pp. 1–12, doi: 10.1061/40940(307)25.

[8] H. Michalak and P. Przybysz, "Subsoil movements forecasting using 3D numerical modeling", *Archives of Civil Engineering*, vol. 67, no. 1, pp. 367–385, 2021, doi: 10.24425/ace.2021.136478.

[9] E.M. Comodromos, M.C. Papadopoulou, and G.K. Konstantinidis, "Effects from diaphragm wall installation to surrounding soil and adjacent buildings", *Computers and Geotechnics*, vol. 53, pp. 106–121, 2013, doi: 10.1016/j.compgeo.2013.05.003.

[10] J. Ko, J. Cho, and S. Jeong, "Nonlinear 3D interactive analysis of superstructure and piled raft foundation", *Engineering Structures*, vol. 143, pp. 204–218, 2017, doi: 10.1016/j.engstruct.2017.04.026.

[11] K. Nepelski, "3D FEM Analysis of the Subsoil-Building Interaction", *Applied Sciences*, vol. 12, no. 21, 2022, doi: 10.3390/app122110700.

[12] C.Y. Ou, Y.L. Lin, and P.G. Hsieh, "Case record of an excavation with cross walls and buttress walls", *Journal of GeoEngineering*, vol. 1, no. 2, pp. 79–86, 2006, doi: 10.6310/jog.2006.1(2).4.

[13] P.G. Hsieh, C.Y. Ou, and Y.L. Lin, "Three-dimensional numerical analysis of deep excavations with cross walls", *Acta Geotechnica*, vol. 8, no. 1, pp. 33–48, 2013, doi: 10.1007/s11440-012-0181-8.

[14] G.B. Liu, P. Huang, J.W. Shi, and C.W.W. Ng, "Performance of a deep excavation andits effect on adjacent tunnels in Shanghai soft clay", *Journal of Performance of Constructed Facilities*, vol. 30, no. 6, 2016, doi: 10.1061/(ASCE)CF.1943-5509.0000891.

[15] A. Lim, P.G. Hsieh, and C.Y. Ou, "Evaluation of buttress wall shapes to limit movements induced by deep excavation", *Computer and Geotechnics*, vol. 78, pp. 155–17, 2016, doi: 10.1016/j.compgeo.2016.05.012.

[16] A. Lim, C.Y. Ou, and P.G. Hsieh, "Investigation of the integrated retaining system to limit deformations induced by deep excavation", *Acta Geotechnica*, vol. 13, no. 4, pp. 973–995, 2018, doi: 10.1007/s11440-017-0613-6.

[17] P.G. Hsieh and C.Y. Ou, "Mechanism of buttress walls in restraining the wall deflection caused by deep excavation", *Tunnelling and Underground Space Technology*, vol. 82, pp. 542–553, 2018, doi: 10.1016/j.tust.2018.09.004.

[18] T. Schanz, P.A. Vermeer, and P.G. Bonnier, "The hardening soil model: formulation and verification", in *Beyond 2000 in Computational Geotechnics – 10 Years Plaxis*. Routledge, 1999, pp. 281–296, doi: 10.1201/9781315138206-27.

[19] A. Lim, C.Y. Ou, and P.G. Hsieh, "Evaluation of clay constitutive models for analysis of deep excavation under undrained conditions", *Journal of GeoEngineering*, vol. 5, no. 1, pp. 9–20, 2010, doi: 10.6310/jog.2010.5(1).2.

[20] M. Calvello and R. Finno, "Selecting parameters to optimize in model calibration by inverse analysis", *Computers and Geotechnics*, vol. 31, no. 5, pp. 410–424, 2004, doi: 10.1016/j.compgeo.2004.03.004.

[21] B.C.B. Hsiung, K.H. Yang, W. Aila, and L. Ge, "Evaluation of the wall deflections of a deep excavation in Central Jakarta", *Tunnelling and Underground Space Technology*, vol. 72, pp. 84–96, 2018, doi: 10.1016/j.tust.2017.11.013.

[22] K.Y. Yong, "Learning lessons from the construction of Singapore buttress wall, colluvial soil, deep excavation, numerical analysis, limiting wall deformationDowntown line (DTL)", presented at International Conference and Exhibition on Tunneling and Underground Space, 2015.

[23] ACI Committee 318, *Building Code Requirements for Structural Concrete (ACI 318-95) and Commentary (ACI 318R-95)*. American Concrete Institute (ACI), 1995, doi: 10.14359/51716937.

[24] A.T.C. Goh, F. Zhang, W. Zhang, Y. Zhang, and H. Liu, "A simple estimation model for 3D braced excavation wall deflection", *Computers and Geotechnics*, vol. 83, pp. 106–113, 2017, doi: 10.1016/j.compgeo.2016.10.022.

[25] C.Y. Ou, P.G. Hsieh, and D.C. Chiou, "Characteristics of ground surface settlement during excavation", *Canadian Geotechnical Journal*, vol. 30, no. 5, pp. 758–767, 1993, doi: 10.1139/t93-068.

Received: 2023-09-11, Revised: 2023-12-12